Mechanical properties of silicon nanobeams with an undercut evaluated by combining the dynamic resonance test and finite element analysis*

Zhang Jia-Hong(张加宏)[a)b)†], Mao Xiao-Li(冒晓莉)[a)b)], Liu Qing-Quan(刘清惓)[a)b)], Gu Fang(顾 芳)[c)], Li Min(李 敏)[a)b)], Liu Heng(刘 恒)[a)b)], and Ge Yi-Xian(葛益娴)[a)b)]

[a)] *Jiangsu Key Laboratory of Meteorological Observation and Information Processing, Nanjing University of Information Science & Technology, Nanjing* 210044, *China*

[b)] *College of Electronic & Information Engineering, Nanjing University of Information Science & Technology, Nanjing* 210044, *China*

[c)] *College of Physics & Opto-Electronic Engineering, Nanjing University of Information Science & Technology, Nanjing* 210044, *China*

(Received 6 December 2011; revised manuscript received 3 February 2012)

Mechanical properties of silicon nanobeams are of prime importance in nanoelectromechanical system applications. A numerical experimental method of determining resonant frequencies and Young's modulus of nanobeams by combining finite element analysis and frequency response tests based on an electrostatic excitation and visual detection by using a laser Doppler vibrometer is presented in this paper. Silicon nanobeam test structures are fabricated from silicon-on-insulator wafers by using a standard lithography and anisotropic wet etching release process, which inevitably generates the undercut of the nanobeam clamping. In conjunction with three-dimensional finite element numerical simulations incorporating the geometric undercut, dynamic resonance tests reveal that the undercut significantly reduces resonant frequencies of nanobeams due to the fact that it effectively increases the nanobeam length by a correct value ΔL, which is a key parameter that is correlated with deviations in the resonant frequencies predicted from the ideal Euler–Bernoulli beam theory and experimentally measured data. By using a least-square fit expression including ΔL, we finally extract Young's modulus from the measured resonance frequency versus effective length dependency and find that Young's modulus of a silicon nanobeam with 200-nm thickness is close to that of bulk silicon. This result supports that the finite size effect due to the surface effect does not play a role in the mechanical elastic behaviour of silicon nanobeams with thickness larger than 200 nm.

Keywords: silicon nanobeams with undercut, mechanical properties, mechanical testing, finite element method

PACS: 61.46.Km, 62.25.–g, 81.70.Bt, 02.70.Dh **DOI:** 10.1088/1674-1056/21/8/086101

1. Introduction

Single crystal silicon (Si) is a most important and common material for very large scale integrated circuits, memory devices, and microelectromechanical systems (MEMSs) due to its unique electronic, thermal, mechanical, and electromechanical properties. With the rapid advances in nanoscience and nanotechnology, the dimensions of these Si-based devices and systems have been pushed to the nanometer scale. For example, the size of MEMS approaches to the size of nanoelectromechanical system (NEMS).[1] In this case, Si nanostructures such as Si nanobeams (SiNBs) and Si nanowires (SiNWs) naturally become the key building blocks for NEMS applications such as high frequency mechanical resonators[2] and ultrasensitive force or mass sensors.[3,4] Obviously, in order to make these applications reliable, the exact evaluation of the size effect on the physics properties of SiNBs and SiNWs is essential and critical. It is noted that nanoscale materials and structures

*Project supported by the National Natural Science Foundation of China (Grant Nos. 41075026 and 61001044), the Open Research Fund of Key Laboratory of Microelectromechanical System of Ministry of Education, Southeast University, China (Grant Nos. 2009-03 and 2010-02), the Special Fund for Meteorology Research in the Public Interest, China (Grant No. GYHY200906037), and the Priority Academic Program Development of Sensor Networks and Modern Meteorological Equipment of Jiangsu Provincial Higher Education Institutions.

†Corresponding author. E-mail: zjhnuist@yahoo.cn

© 2012 Chinese Physical Society and IOP Publishing Ltd

serving as electrical components of NEMS are attributed mainly to their potential remarkable mechanical properties. Thus, the exploration of the changes of mechanical properties, especially Young's modulus of silicon on the nanometer scale is of prime importance in application to the NEMS. Considerable efforts have been made to evaluate the mechanical properties of Si nanostructures experimentally.[5] At present, several approaches and techniques have been developed to measure the mechanical behaviours of Si nanostructures, such as measuring uniaxial tensions of suspended SiNWs in transmission or scanning electron microscopes (TEM/SEM),[6,7] measuring the lateral bendings of suspended SiNBs and SiNWs with an atomic force microscope (AFM),[8−13] observing the resonances of the SiNBs and SiNWs by using a laser vibrometer,[14−16] nanoindentation of SiNBs on a substrate,[17,18] and measuring the pull-in voltage by using the electrostatic pull-in instability method.[19,20] And then, in conjunction with some empirical formulas, Young's modulus of Si nanostructure can be indirectly extracted.

However, on the one hand, available experimental results on SiNBs and SiNWs exhibit significant scatter. Some investigations showed that Young's modulus decreases with size narrowing,[6,7,14,18−20] while the other studies reported an opposite trend,[10−12,15] and another conclusion that Young's modulus of Si nanostructure is close to that of bulk silicon.[8,9,13,16,17] In particular, even if the Young's modulus of the Si nanostructure has the same trend with the size decreasing, the magnitudes of change in different experiments are significantly different from each other. The above results occur mainly because of the following fact that the experimental results include considerable uncertainties and errors, especially in high surface-to-volume ratio Si nanostructures, such as uncertainties and errors from difficulties in measuring real deflection, determining contact area and position and preventing tip slippage in static bending tests with AFM,[12,21] uncertainties and errors from the uncertainty of boundary conditions and the effects of extra surface mass due to native oxide, surface contaminations and other adsorbed layers in dynamic resonance test,[22,23] uncertainties and errors from determining the geometry sizes of nanostructures and the pull-in voltage in electrostatic pull-in instability method,[19,20] and uncertainties and errors from the effects of fabrication-induced defects and undercut.[20]

On the other hand, we note that although the mechanical properties of SiNBs and SiNWs have been extensively studied as mentioned above, almost all Si nanostructures were fabricated by using non-standard manufacturing processes, such as the vapour–liquid–solid growth process,[7,10−13,15−18] field-enhanced anodization using AFM,[8,14] and electron beam lithography,[9] and only limited information is available about the mechanical properties of SiNBs fabricated by standard complementary metal–oxide–semiconductor (CMOS) manufacturing technology,[19,20] and understanding of the effects of fabrication-induced defects and undercut involved in post-CMOS process on the mechanical properties of Si nanostructures is lacking at present. Therefore, from the perspective of large-scale production, it is necessary and meaningful to study the influences of defects and undercuts involved in the post-CMOS process on the mechanical properties of Si nanostructures. In other words, in order to exactly detect the mechanical properties of Si nanostructures with defects and undercut, more reliable experimental research should be carried out.

It is worth noting that the combined methods which rely on the modeling of the beam geometry by a finite element (FE) analysis together with experimentally frequency response test have received more and more attention,[24−28] and there has been a tendency to determine the resonant frequency and Young's modulus of the nanostructure and the undercut effect by using this combined method. Specifically, Gavan *et al.*[24] have recently adopted this combined method to study the effect of undercut induced by an isotropic dry etch process on the resonant behaviour of silicon nitride cantilever. Guillon *et al.*[25] explored the effects of non-ideal clamping shape on the resonance frequency of a silicon nanocantilever. More recently, Nazeer *et al.*[26] investigated the influences of silicon orientation and cantilever undercut on the determination of the Young's modulus of PZT thin film. Ilic *et al.*[27] have presented an accurate combined method of simultaneously measuring Young's modulus and density of thin alumina, hafnia, and aluminum nitride nanofilms by using in-plane and out-of-plane vibration modes of nanomechanical cantilevers. In a recent report, a numerical–experimental combined approach to the measurement of the effective Young's modulus and its size effect in homogeneous Cu nanofilm has also been demonstrated.[28]

In the present paper, we present a versatile numerical experimental combined method of determining resonant frequency and Young's modulus of SiNB by combining FE analysis and frequency response

tests based on an electrostatic excitation and visual detection by using a laser Doppler vibrometer. The SiNBs are fabricated from (100) silicon-on-insulator wafers by using the SMIC 0.18-μm CMOS process, and we focus on investigating the influence of undercut caused by overetching during final wet release process on mechanical properties of the SiNBs. In order to obtain accurate and reliable measurements in this kind of method, detection of Young's modulus involves three steps: the first step is to detect the fundamental resonant frequency by an experimental resonance method and to extract Young's modulus from the measured data by performing a least-square fit through a corrected Euler–Bernoulli beam formula. The second step is to model the frequency response and to extract Young's modulus from the simulated fundamental resonant frequency by performing a least-square fit through the corrected Euler–Bernoulli beam formula. The last step is to compare experimental results in the first step and FE numerical simulation results in the second step to determine the practical Young's modulus.

2. Experimental details

2.1. Fabrication of single-crystal SiNBs with undercut

Based on the SMIC 0.18-μm CMOS process, the single and double clamped SiNBs (nanocantilevers and nanobridges) with same thickness (t) were fabricated from (100) silicon-on-insulator wafers with a 200-nm buried oxide (BOX) and a 200-nm single-crystal silicon surface device layer, respectively. The first step of fabrication process was to determine the patterns of ⟨110⟩ oriented SiNBs of different lengths (L) and widths (w) onto silicon surface device layer by standard photolithography. After this, reactive ion etchings were used to etch the silicon device layer and the exposed BOX until the silicon substrate. Then heavily doped p-type layer was formed in the anchor region, followed by sputtering 600-nm Al metal as top electrode (pad). A photoresist was then spinned in the metal pad region in order to prevent corrosion of Al metal in the release process of SiNBs. Finally, the BOX underneath SiNBs was etched using a buffered oxide etcher (BOE) solution and SiNBs were then released using critical point drying in liquid carbon dioxide (post-CMOS process).[29] In general, the SiNB test structures released in this way do not collapse, and the above method for the suspended SiNBs is a CMOS–MEMS process.

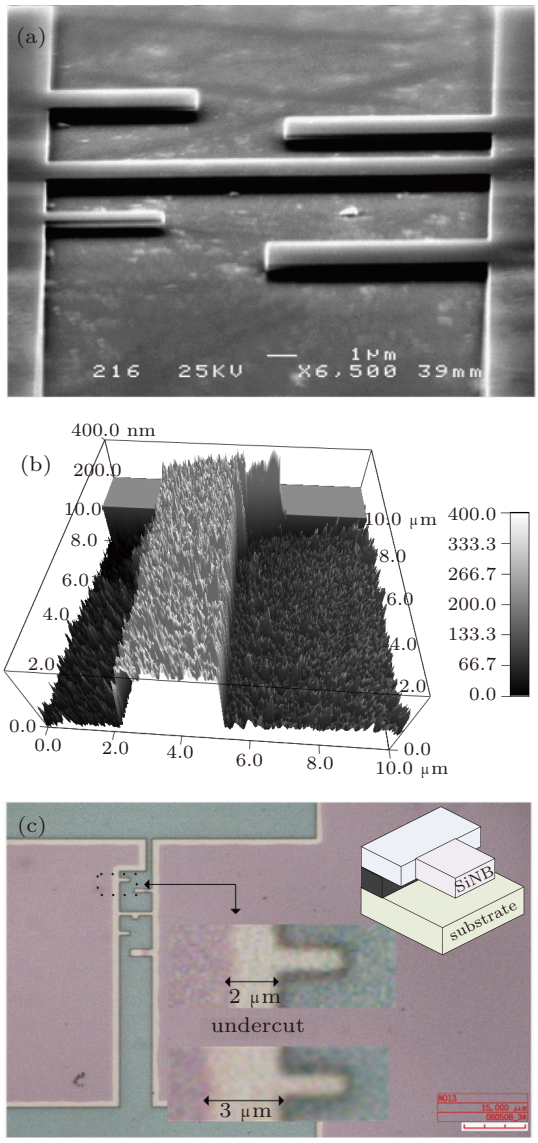


Fig. 1. (colour online) SEM micrograph (a), AFM scanning image (b), optical microscope image (c) of the SiNB fabricated by using a CMOS–MEMS process. The optical micrograph clearly shows that the base of the SiNB is overetched. The white strip near the base of the nanobeam indicates the undesired undercut, and the scale bar corresponds to 15 μm. Inset in panel 1(c) shows a schematic profile view of the clamp region of a nanobeam with undercut, and the black block represents the BOX.

Figure 1(a) shows an SEM micrograph of SiNBs after the final release process, and Fig. 1(b) illustrates an AFM micrograph of an SiNB. From SEM and AFM micrographs, we can accurately determine the sizes of SiNBs. Note that the excessive etching of the BOX below the anchor area is difficult to avoid in post-CMOS process, which inevitably generates the undercut of the nanobeam clamping (the overhanging at nanobeam clamping). This undercut can affect

the mechanical characteristics. For example, the resonance frequency may be shifted towards lower values because of the increase in effective length of the nanobeam, which reduces the spring constant.[24,25] Fortunately, this undercut can be measured by optical microscopy as can be seen from Fig. 1(c), and the obvious 2-μm or 3-μm long undercut caused by overetching may be introduced at the base of the SiNBs in our final wet release process, and the length of the undercut depends on nanobeam width, etch time, etch rate, etc.[27,28] In order to visually reflect the actual situation of the underetched nanobeam, a schematic profile view of the clamp region of a nanobeam with undercut is also shown in the inset of Fig. 1(c). As we can see, the BOX below the anchor area is excessively etched.

2.2. Dynamic resonance test with an LDV measurement setup

The schematic plot of the polytec laser Doppler vibrometer (LDV) measurement setup is sketched in Fig. 2. The out-of-plane resonance of the SiNB is excited by an AC signal ($V_{\rm ac}$) riding on the DC bias voltage ($V_{\rm dc}$). The AC bias voltage is a periodic chirp signal whose amplitude ranges from 0 to 10 volt, and the strength of excitation signal is selectively chosen to avoid being submerged by noise and generating nonlinear resonant effect. As can be seen from Fig. 2, under the electrostatic excitation in the drive mode, the out-of-plane resonant behaviours of SiNBs were measured in air by using LDV optical detection method,[30] which can work at high-precision non-contact mode, and can receive real-time images of the vibration mode through CCD camera as shown in Figs. 3(a) and 3(b), which can be used to easily and accurately determine the fundamental resonant mode of the SiNB. As can also be seen from Figs. 3(a) and 3(b), the overhanging at nanobeam clamping participates in the resonance, which will inevitably affect the resonant characteristics of SiNBs.

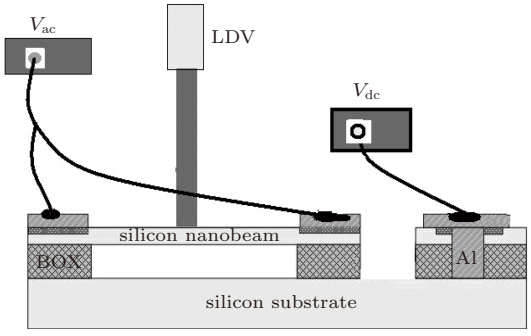


Fig. 2. Schematic plot of LDV measurement setup for dynamic resonance test.

In the LDV measurement setup, in order to accurately observe the amplitude-frequency of the SiNB, optimally adjusting the laser spot position to select the maximum amplitude (the free end of the nanocantilever or the mid-point of the nanobridge) as measurement point is also a critical issue. Figures 3(c) and 3(d) show the amplitude-frequency relations of a nanocantilever and nanobridge measured by using LDV. For a nanocantilever with dimensions $L\times w\times t =$ 5 μm × 1.5 μm × 0.2 μm, the measured fundamental frequency is about 8.1 MHz, and for a nanobridge $L \times w \times t = 12$ μm × 3 μm × 0.2 μm, its fundamental frequency is about 6.7 MHz. However, based on the Euler–Bernoulli beam model, their fundamental frequencies are about 11.1 MHz and 12.2 MHz, respectively, which shows that the undercut significantly reduces the resonant frequencies of SiNBs. In addition, as shown in Figs. 3(c) and 3(d), the maximum amplitude is just a few tenths of nanometers, which makes it sure that the deformation of the SiNB is elastic and it vibrates within the linear elastic range.

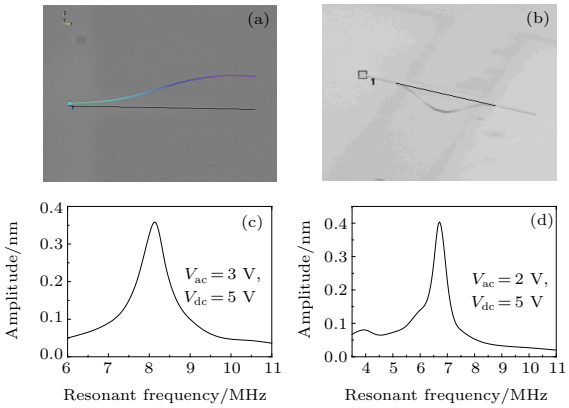


Fig. 3. (a) Vibration pattern of the silicon nanocantilever when scanning the phase, (b) vibration pattern of the silicon nanobridge when scanning the phase, (c) amplitude–frequency relation of the silicon nanocantilever, (d) amplitude–frequency relation of the silicon nanobridge.

3. Theoretical analysis for the fit formula with the correction length

This analysis intends to investigate the relation between the extracted Young's modulus and the measured fundamental frequencies of the SiNBs with undercut using an LDV optical detection method, which will serve as the fit formula for the extraction of material parameters, such as the Young's modulus. On the one hand, according to the vibration analysis of an Euler–Bernoulli beam model based on the ideal

boundary conditions,[31,32] the Young's modulus E and the fundamental resonant frequency of the bending vibration f_0 of the beam without undercut has the following relationship:

$$f_0 = \frac{\lambda^2 t}{4\pi L^2}\sqrt{\frac{E}{3\rho}} \qquad \text{(cantilever)}, \tag{1}$$

$$f_0 = \frac{\eta^2 \pi t}{4L^2}\sqrt{\frac{E}{3\rho}} \qquad \text{(bridge)}, \tag{2}$$

where $\lambda = 1.875$, $\eta = 1.5$, ρ is the density of silicon, L and t are the length and thickness of the beam, respectively. Equations (1) and (2) clearly show that the relation between resonant frequency and inverse length squared is linear.

On the other hand, according to Ref. [24], the undercut ($L_{\rm u}$) will lead to a deviation from the linear relation between f_0 and L^{-2} predicted by Eqs. (1) and (2). This result occurs because the base region near the anchoring point participates in the overall resonance behaviour of the beam. Apparently, in order to accurately extract the Young's modulus of the SiNB, Eqs. (1) and (2) must be corrected, and the effect of undercut should be included into the beam effective length by adding a correction length ΔL.[24–28] In the case, the effective lengths of the silicon nanocantilever and nanobridge with undercut are given by $L_{\rm eff} = L + \Delta L$ and $L_{\rm eff} = L + 2\Delta L$, respectively, where L is the original beam length and ΔL is the correction length of the undercut. Thus we have

$$f_0 = \frac{\lambda^2 t}{4\pi L_{\rm eff}^2}\sqrt{\frac{E}{3\rho}} = \frac{\lambda^2 t}{4\pi(\Delta L + L)^2}\sqrt{\frac{E}{3\rho}} \qquad \text{(cantilever)}, \tag{3}$$

$$f_0 = \frac{\eta^2 \pi t}{4L_{\rm eff}^2}\sqrt{\frac{E}{3\rho}} = \frac{\eta^2 \pi t}{4(2\Delta L + L)^2}\sqrt{\frac{E}{3\rho}} \qquad \text{(bridge)}, \tag{4}$$

Note that the added length ΔL in Eqs. (3) and (4) is dependent on the length of the undercut but independent of the length of the beam, so the SiNBs with similar widths, which were processed in a similar way, will have the same undercuts and correction lengths.

In short, based on the corrected Euler–Bernoulli theory, i.e., Eqs. (3) and (4), once the dimensions L, t, and the fundamental resonance frequencies of bending mode of the SiNBs with undercut are experimentally determined, by performing a least-square fit through the measured resonance frequency data with ΔL and E used as free parameters in the fitting routine, one can simultaneously extract the correction length ΔL and the Young's modulus E of the SiNBs.

4. Experimental results and discussion

In our numerical experimental–combined method, the first step is to detect the fundamental resonant frequency by a dynamic resonance test and to simultaneously extract Young's modulus and the correction length from the measured resonant frequency data for fabricated SiNBs with a range of length dimensions by performing a least-square fit based on Eqs. (3) and (4). However, in order to test the applicability and adequacy of the ideal Euler–Bernoulli theory, i.e., Eqs. (1) and (2) for the determination of E, we first investigate the dependence of the fundamental resonance frequency f_0 on L^{-2} for SiNB without adding a correction length ΔL. As shown in Figs. 4(a) and 5(a), the observed nonlinear dependence indicates that the undercut leads to a deviation from the linear relation predicted by Eqs. (1) and (2). As analysed above, this result occurs because the base region near the anchoring point participates in the overall resonance behaviour of the SiNB with undercut.

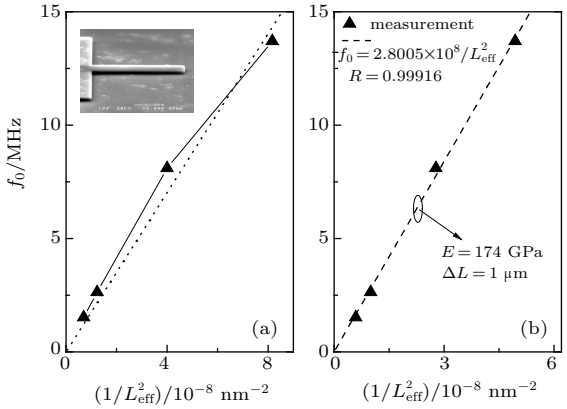


Fig. 4. (a) Fundamental resonance frequency of the bending mode versus $1/L^2$, showing a marked deviation from the expected linear behaviour (dotted linear line is a guide to the eye), (b) fundamental resonance frequency of the bending mode versus $1/L_{\rm eff}^2$. The dashed line shows a fitting straight line. The width and thickness of the silicon nanocantilever is 1.5 μm and 200 nm, respectively, and its length varies from 3.5 μm to 12 μm.

As mentioned previously, the effect of undercut can be included by adding a correction length ΔL ($2\Delta L$) to the nominal length L of the nanocantilever (nanobridge). Thus the effective length of the underetched nanobeam is give by $L_{\rm eff} = L + \Delta L$ ($2\Delta L$). Figure 4(b) shows the fundamental resonance frequency of the bending mode of the silicon nanocantilever versus $1/L_{\rm eff}^2$. The experimental data are linearly fitted by performing a least-square fit (fit function Eq. (3)

passes through zero point) with ΔL and E used as fit parameters, so ΔL and E can be determined simultaneously. Specifically, in order to restore the linear relation between f_0 and $1/(L+\Delta L)^2$, ΔL is determined to be 1 μm for these samples due to the 2-μm undercut. Obviously, linear relationship can be clearly found from the distribution of the measured data points in Fig. 4(b). At this time, the slope of the fitted straight line is 2.8005×10^8 MHz/nm^{-2} and the correlation coefficient R is 0.99916. In this case, based on Eq. (3), the Young's modulus of the silicon nanocantilever, inferred from the slope of the fitting straight line, is 174 GPa. A similar analysis has also been performed on the silicon nanobridges each with undercut of 3 μm as shown in Fig. 5(b), the linear relation between f_0 and $1/L_{\rm eff}^2$ is restored for ΔL equal to 2 μm, and the Young's modulus of the silicon nanobridge, inferred from the slope of the fitting curve, is 177 GPa. In short, the above experimental results show that Young's modulus of the 200-nm thick SiNBs in the ⟨110⟩ direction with different boundary conditions is found to be within 4.2% of the bulk silicon value (170 GPa), which experimentally indicates that finite size effect due to surface effect does not play a role in mechanical behaviours of SiNBs with the thickness larger than 200 nm.

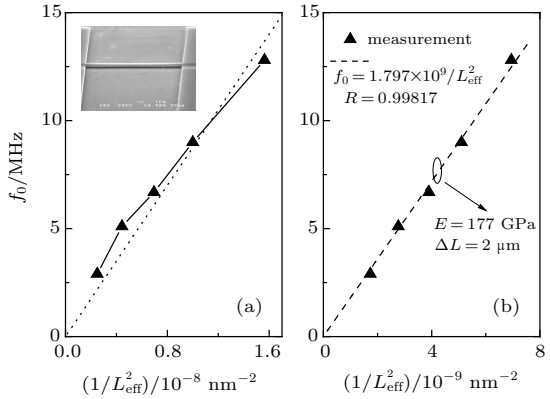


Fig. 5. (a) Fundamental resonance frequency of the bending mode versus $1/L^2$, showing a marked deviation from the expected linear behaviour (dotted linear line denotes a guide to the eye), (b) fundamental resonance frequency of bending mode versus $1/L_{\rm eff}^2$. The dashed line shows the fitting straight line. The width and thickness of the silicon nanobridge are 3 μm and 200 nm, respectively. The length varies from 8 μm to 20 μm.

To further illustrate the importance of introducing the correction length ΔL to include the effect of undercut, Fig. 6 shows Young's moduli of SiNBs with undercut calculated by the ideal Euler–Bernoulli theory (Eqs. (1) and (2)) without considering undercut and the corrected Euler–Bernoulli theory (Eqs. (3) and (4)) with considering undercut as well as the fitting result. As can be seen from Fig. 6, Eqs. (1) and (2) give the very low Young's moduli in a range from 35 GPa to 105 GPa. Obviously, Young's moduli calculated by Eqs. (1) and (2) are underestimated because of the fact that in the specific calculation, theoretical design length (the original beam length L) is kept the same, but the actual resonant frequency significantly decreases due to stiffness variation at the clamped end, caused by the undercut. On the other hand, after we introduce the correction length ΔL, the Young's moduli calculated by using Eqs. (3) and (4) vary in a range from 142 GPa to 188 GPa, which is close to that of bulk silicon. Based on previous studies,[8,9] these values are rational, which shows that the correction length ΔL must be introduced when we analyse the mechanical properties of SiNBs with undercut.

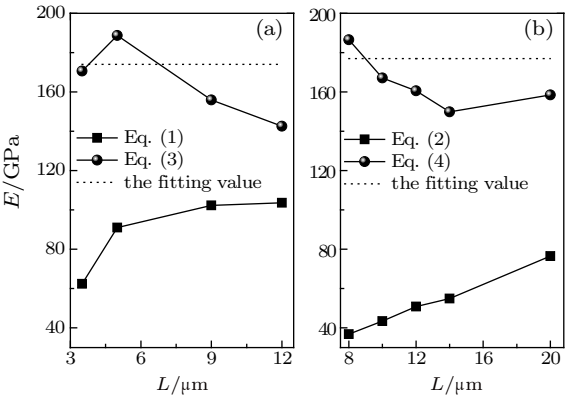


Fig. 6. (a) Young's moduli of silicon nanocantilevers with undercut versus their original length calculated by the different calculation formulas, (b) Young's moduli of silicon nanobridges with undercut versus their original length calculated by the different calculation formulas.

5. Numerical simulations and comparison with measurements

In our combined numerical and experimental method, the second step is to model the frequency response of the nanobeam with undercut and to extract Young's moduli from the simulated fundamental resonant frequency by performing a least-square fit through Eqs. (3) and (4). A three-dimensional FE simulation is carried out for the fundamental resonant frequency using ANSYS. As in the ANSYS input parameters are assumed, the experimental value

for the mass density (2330 kg/m^3) is used whereas the Young's modulus (170 GPa) and Poisson's ratio (0.064) are taken from Ref. [26]. In order to investigate the influence of undercut arising from the wet chemical release process of the nanomechanical structure, the underetched nanobeam is modeled as a stepped beam as illustrated in Figs. 7(a) and 7(b). Note that the FE simulations show that if the width of the plate is greater than 15 μm, then the influence of the width on simulation result is very small. Because the width of anchor plate in our experiment is generally greater than 20 μm, the influence of the width can be neglected. In the specific simulation, the nanocantilever is attached to the 2-μm long and 15-μm wide plate, and the nanobridge is attached to the 3-μm long and 20-μm wide plates. Three lateral edges of the plate are clamped, while the nanobeam is attached to the free edge. Moreover, released areas of nanobeam and underetched base regions (plate with three clamped lateral edges) are allowed to move freely in the FE simulation. In this case, FE results are uniquely determined. Figures 7(c) and 7(d) illustrate the vibration mode dependence on the stress distribution in close proximity to the clamped end of the nanobeam. The simulations show that the stress propagation into the overhang region is significant, which numerically reveals that the undercut inevitably affects the mechanical resonant characteristics of SiNBs.

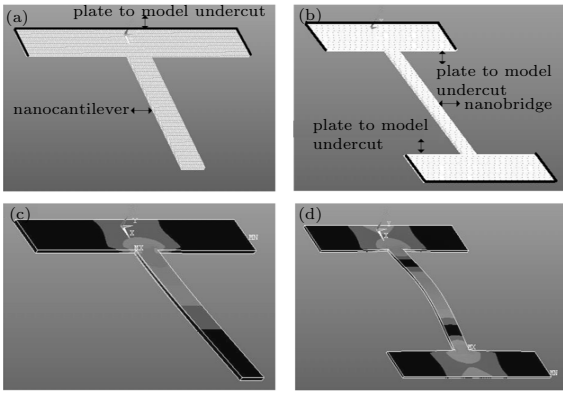


Fig. 7. (a) Three-dimensional FE mesh of the silicon nanocantilever. The 9-μm long, 1.5-μm wide, and 200-nm thick cantilever is attached to a 2-μm long, 15-μm wide plate emulating the undercut. Highlighted edges represent three clamped lateral edges of the plate, (b) three-dimensional FE mesh of the silicon nanobridge. The 12-μm long, 2-μm wide, and 200-nm thick bridge is attached to the 3-μm long, 20-μm wide plates emulating the undercuts. (c) FE simulation of the vibration mode dependence on the stress distribution near the single clamped end of the silicon nanocantilever, (d) FE simulation of the vibration mode dependence on the stress distribution near the double clamped end of the silicon nanobridge.

Figures 8(a) and 8(c) show the comparisons between the measured and simulated resonance frequencies of the SiNBs. The triangles, squares, and circles represent the measured and simulated data with and without undercut, respectively. As expected, on the one hand, resonance frequencies obtained from the FE simulations without undercut are much larger than those from the measurements and the FE simulations with undercut, which reveals that the undercut significantly reduces resonant frequencies due to the fact that it effectively increases the nanobeam length by a correct value ΔL. Thus, ΔL is a key parameter that is correlated with deviations in the resonant frequencies predicted from the ideal Euler–Bernoulli beam theory and experimental measured data. On the other hand, the FE simulations with undercut correspond rather well to the experimentally measured resonance frequencies for the range of nanobeam length, i.e., the FE simulations with undercut can basically reproduce the relation between experimental frequency and L^{-2}. By using the least square method, we extract the simulated correction to the nominal length and Young's moduli for the two different boundary conditions as shown in Figs. 8(b) and 8(d). The determined Young's moduli from the fitting routine are 171 GPa for the nanocantilever and 175 GPa for the nanobridge, respectively. Obviously, a good agreement between the FE calculated and assumed values of Young's modulus is observed. Compared with the assumed value (170 GPa), the relative error of the FE calculated Young's modulus is less than a few percent.

The last step is to compare experimental results in the first step and numerical simulation results in the second step to determine the practical Young's modulus. Experimental results and simulation results are presented in Table 1. It is found that experimental results for SiNBs are in excellent agreement with the three-dimensional FE analysis. For the silicon nanocantilever, a 1.7% variation between the Young's modulus from the FE simulation results and that from experimental results is observed. For the silicon nanobridge, the relative error is only 1.1%. Thus, the practical Young's modulus of the SiNBs is determined to be indeed about 170 GPa, which shows that Young's modulus of the SiNB with 200-nm thickness remains that of bulk silicon. This result supports that finite size effect due to surface effect does not play a role in mechanical elastic behaviour of the SiNBs with the thickness larger than 200 nm.

Table 1. Comparison between Young's modulus extracted from measured resonant frequencies (E^{M}) and that from FE simulated resonant frequencies (E^{FE}) for the silicon nanocantilever and silicon nanobridge, respectively. Young's modulus is in GPa.

SiNB	E^{M}	E^{FE}	$(E^{\mathrm{FE}} - E^{\mathrm{M}})/E^{\mathrm{M}}$
Nanocantilever	174	171	1.7%
Nanobridge	177	175	1.1%

It is also important to note that numerical and experimental results are well consistent with each other in this paper. However, if the two are inconsistent then one needs further analysis and simulation to determine which one will prevail. In general, the ANSYS FE simulation results are relatively reliable because the FE method has been regarded as design and verification method in a lot of literature. However, in some cases, we cannot say that the FE result is completely correct and effective. For example, if experimental test structures contain surface stress or residual stress, but FE method does not contain these factors and then the two results are inconsistent. In this case, the FE method needs to contain the effect of the stress and re-simulate, and then the simulation and experimental results are likely to coincide with each other.

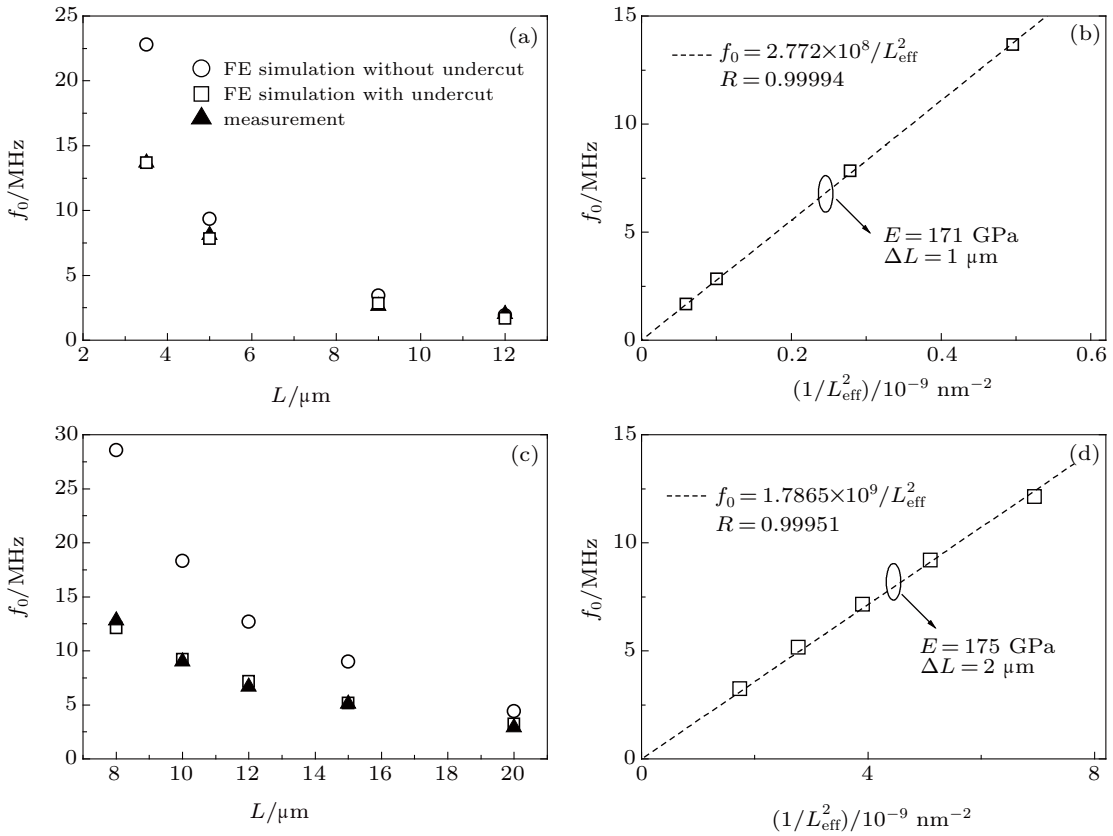


Fig. 8. (a) Comparisons between the measured and FE simulated resonant frequencies of silicon nanocantilevers with and without undercut, (b) Young's modulus and the correction length of silicon nanocantilevers are obtained by fitting the resonance frequency data points from FE numerical simulations, (c) comparison between the measured and the FE simulated resonant frequencies of silicon nanobridges with and without undercut, (d) Young's modulus and the correction length of silicon nanobridges are obtained by fitting the resonance frequency data points from FE numerical simulations.

6. Conclusion

In this paper, we demonstrated a combined numerical and experimental method to analyse the vibration of SiNBs with undercut fabricated by using a CMOS–MEMS process and to determine the Young's moduli of SiNBs with a wide range of lengths. In this combined method, we can simultaneously determine the Young's modulus and the correction length of the SiNBs with undercut by performing and comparing a least-square fit through the measured frequency response data combined with the FE numerical simulation data. This combined method is generally applicable for arbitrary beam dimensions. Our research shows that the undercut significantly reduces the res-

onance frequency of the SiNBs because of the increase in their effective length. In this case, based on the ideal Euler–Bernoulli beam theory, we will obtain an erroneous and significantly reduced Young's modulus. However, by introducing a correction length, we can obtain reasonable results for the resonant frequency and Young's modulus of the SiNBs. Finally, our fitting results clearly indicate that the Young's modulus of the SiNB with 200-nm thickness is expected to remain that of bulk silicon. This result supports that the finite size effect due to the surface effect does not play a role in the mechanical elastic behaviour of SiNBs with thicknesses larger than 200 nm. Since the undercut cannot be avoided in the CMOS–MEMS fabrication process, this research might be useful for evaluating the influence of manufacturing process-induced undercut on mechanical properties of the SiNB-based NEMS.

Acknowledgement

The authors are grateful to the Key Laboratory of MEMS, Ministry of Education, Southeast University for post-CMOS wet etching and laser Doppler vibrometer measurements, and also to the SMIC (Shanghai) for providing fabrication facilities.

References

[1] Craighead H G 2000 *Science* **290** 1532

[2] Feng X L, He R R, Yang P D and Roukes M L 2007 *Nano Lett.* **7** 1953

[3] He R R and Yang P D 2006 *Nature Nanotechnology* **1** 42

[4] Gil-Santos E, Ramos D, Martínez J, Fernández-Regúlez M, García R, Paulo Á S, Calleja M and Tamayo J 2010 *Nature Nanotechnology* **5** 641

[5] Jin Q H, Li T, Zhou P and Wang Y L 2009 *J. Nanomater.* **2009** 319842

[6] Kizuka T, Takatani Y, Asaka K and Yoshizaki R 2005 *Phys. Rev.* B **72** 035333

[7] Zhu Y, Xu F, Qin Q, Fung W Y and Lu W 2009 *Nano Lett.* **9** 3934

[8] Namazu T, Isono Y and Tanaka T 2000 *J. Microelectromech. Syst.* **9** 450

[9] Virwani K R, Malshe A P, Schmidt W F and Sood D K 2003 *Smart. Mater. Struct.* **12** 1028

[10] Paulo A S, Bokor J, Howe R T, He R, Yang P, Gao D, Carraro C and Maboudian R 2005 *Appl. Phys. Lett.* **87** 053111

[11] Heidelberg A, Ngo L T, Wu B, Phillips M A, Sharma S, Kamins T I, Sader J E and Boland J J 2006 *Nano Lett.* **6** 1101

[12] Gordon M J, Baron T, Dhalluin F, Gentile P and Ferret P 2009 *Nano Lett.* **9** 525

[13] Hsin C L, Mai W J, Gu Y D, Gao Y F, Huang C T, Liu Y Z, Chen L J and Wang Z L 2008 *Adv. Mater.* **20** 3919

[14] Li X X, Ono T, Wang Y L and Esashi M 2003 *Appl. Phys. Lett.* **83** 3081

[15] Tabib-Azar M, Nassirou M, Wang R, Sharma S, Kamins T I, Islam M S and Williams R S 2005 *Appl. Phys. Lett.* **87** 113102

[16] Belov M, Quitoriano N J, Sharma S, Hiebert W K, Kamins T I and Evoy S 2008 *J. Appl. Phys.* **103** 074304

[17] Sohn Y S, Park J, Yoon G, Song J, Jee S W, Lee J H, Na S, Kwon T and Eom K 2010 *Nanoscale Res. Lett.* **5** 211

[18] Stan G, Krylyuk S, Davydov A V and Cook R F 2010 *Nano Lett.* **10** 2031

[19] Sadeghian H, Yang C K, Goosen J F L, van der Drift E, Bossche A, French P J and van Keulen F 2009 *Appl. Phys. Lett.* **94** 221903

[20] Sadeghian H, Yang C K, Goosen J F L, Bossche A, Staufer U, French P J and van Keulen F 2010 *J. Micromech. Microeng.* **20** 064012

[21] Agrawal R, Peng B, Gdoutos E E and Espinosa H D 2008 *Nano Lett.* **8** 3668

[22] Ding W, Calabri L, Chen X, Kohlhaas K M and Ruoff R S 2006 *Compos. Sci. Technol.* **66** 1112

[23] Craighead H 2007 *Nature Nanotechnol.* **2** 18

[24] Gavan K B, van der Drift E W J M, Venstra W J, Zuiddam M R and van der Zant H S J 2009 *J. Micromech. Microeng.* **19** 035003

[25] Guillon S, Saya D, Mazenq L, Perisanu S, Vincent P, Lazarus A, Thomas O and Nicu L 2011 *Nanotechnology* **22** 245501

[26] Nazeer H, Woldering L A, Abelmann L, Nguyen M D, Rijnders G and Elwenspoek M C 2011 *Microelectron. Eng.* **88** 2345

[27] Ilic B, Krylov S and Craighead H G 2010 *J. Appl. Phys.* **108** 044317

[28] Poelma R H, Sadeghian H, Noijen S P M, Zaal J J M and Zhang G Q 2011 *J. Micromech. Microeng.* **21** 065003

[29] Jenkins N E, DeFlores L P, Allen J, Ng T N, Garner S R, Kuehn S, Dawlaty J M and Marohn J A 2004 *J. Vac. Sci. Technol.* B **22** 909

[30] Chen J, Qin M and Huang Q A 2011 *Chin. Phys.* B **20** 097101

[31] Park H 2008 *J. Appl. Phys.* **103** 123504

[32] Zhang J H, Li M, Gu F and Liu Q Q 2012 *Chin. Phys.* B **21** 016203